Spectroscopic measurements of tropospheric CO, C_2H_6, C_2H_2, and HCN in northern Japan

Y. Zhao,[1,2] K. Strong,[1] Y. Kondo,[3] M. Koike,[4] Y. Matsumi,[5] H. Irie,[5] C. P. Rinsland,[6] N. B. Jones,[7] K. Suzuki,[8] H. Nakajima,[9] H. Nakane,[9] and I. Murata[10]

Received 19 April 2001; revised 16 October 2001; accepted 18 October 2001; published 17 September 2002.

[1] Tropospheric column amounts and mixing ratios of CO, C_2H_6, C_2H_2, and HCN were retrieved from ground-based infrared solar spectra using a vertical profile retrieval algorithm (SFIT2). The spectra were recorded with high spectral resolution Fourier transform infrared (FTIR) spectrometers at Moshiri (44.4°N) and Rikubetsu (43.5°N) in northern Japan from May 1995 to June 2000. The retrievals show significant seasonal variations in the tropospheric content of the four molecules over northern Japan with maxima in winter-spring (February–April) for CO, C_2H_6, and C_2H_2 and in summer (May–July) for HCN. Good correlations between CO, C_2H_6, and C_2H_2 indicated that they had similar sources and underwent similar dilution processes. Deviation of HCN relative to its seasonal mean value (ΔHCN) is correlated with the similar deviation of CO (ΔCO), indicating that enhancements of CO and HCN above the mean levels were probably due to the same sources. Linear trends in tropospheric CO, C_2H_6, and C_2H_2 from May 1995 to June 2000 (excluding 1998) were (-2.10 ± 0.30), (-2.53 ± 0.30), and (-3.99 ± 0.57)%/yr, respectively, while the trend of (-0.93 ± 0.49)%/yr in HCN was relatively small. Abnormally high tropospheric amounts of the four molecules were recorded in 1998. HCN amounts were found to be much higher than its seasonal mean value throughout 1998 with a 65% maximum increase in August 1998. Significant increases of CO, C_2H_6, and C_2H_2 took place in August–October 1998. Trajectory calculations, global fire maps, and satellite smoke images revealed that biomass burning in eastern Siberia from mid-July to early October 1998 was the major cause of the elevated levels in tropospheric CO, C_2H_6, C_2H_2, and HCN observed in northern Japan in 1998. *INDEX TERMS:* 0322 Atmospheric Composition and Structure: Constituent sources and sinks; 0345 Atmospheric Composition and Structure: Pollution—urban and regional (0305); 0365 Atmospheric Composition and Structure: Troposphere—composition and chemistry; 0368 Atmospheric Composition and Structure: Troposphere—constituent transport and chemistry; *KEYWORDS:* infrared, remote sensing, tropospheric species, biomass burning

Citation: Zhao, Y., et al., Spectroscopic measurements of tropospheric CO, C_2H_6, C_2H_2, and HCN in northern Japan, *J. Geophys. Res.*, *107*(D18), 4343, doi:10.1029/2001JD000748, 2002.

[1]Department of Physics, University of Toronto, Toronto, Canada.
[2]Now at Mechanical and Aeronautical Engineering, University of California, Davis, California, USA.
[3]Research Center for Advanced Science and Technology, University of Tokyo, Tokyo, Japan.
[4]Department of Earth and Planetary Sciences, Graduate School of Science, University of Tokyo, Tokyo, Japan.
[5]Solar-Terrestrial Environment Laboratory, Nagoya University, Toyokawa, Japan.
[6]Atmospheric Sciences Division, NASA Langley Research Center, Hampton, Virginia, USA.
[7]National Institute of Water and Atmospheric Research, Lauder, New Zealand.
[8]Faculty of Education and Human Sciences, Yokohama National University, Yokohama, Japan.
[9]National Institute of Environmental Studies, Tsukuba, Japan.
[10]Department of Astronomy and Geophysics, Graduate School of Science, Tohoku University, Sendai, Japan.

0148-0227/02/2001JD000748$09.00

1. Introduction

[2] Carbon monoxide (CO), ethane (C_2H_6), and acetylene (C_2H_2) are important tropospheric ozone (O_3) precursors. Changes in the tropospheric concentration of these molecules could affect the regional and global tropospheric O_3 budget. High tropospheric O_3 due to biomass burning in southeast Asia was observed by ozonesondes in Hong Kong (22.2°N, 114.3°E) in April 1994, coinciding with the dry season in southeast Asia [*Chan et al.*, 2000]. Biomass burning is a significant source of tropospheric CO, nonmethane hydrocarbons (NMHCs), and hydrogen cyanide (HCN). As biomass burning products, CO, C_2H_6, C_2H_2, and HCN have been observed in the field and in laboratory fire experiments [*Yokelson et al.*, 1996, 1997; *Holzinger et al.*, 1999]. In addition, combustion of fossil fuel and oxidation of methane (CH_4) and NMHCs also provide important sources for tropospheric CO. Natural gas and automobile emissions are important sources of C_2H_6 and C_2H_2, respec-

tively [*Logan et al.*, 1981; *Singh and Zimmerman*, 1992; *Rudolph*, 1995]. Major sinks of tropospheric CO, C_2H_6, and C_2H_2 are reactions with the hydroxyl radical (OH) [*Logan et al.*, 1981; *Singh and Zimmerman*, 1992]. Tropospheric lifetimes of CO, C_2H_6, and C_2H_2 vary with season and latitude, and the global averages are ~2 months for both CO and C_2H_6 and ~1 month for C_2H_2 [*Logan et al.*, 1981; *Volz et al.*, 1981; *Singh and Zimmerman*, 1992; *Gupta et al.*, 1998]. Owing to the relatively short tropospheric lifetimes, spatial and temporal variations in the concentrations of these three molecules contain important information on their sources, sinks, and transport. The principle pathway for HCN loss was initially suggested to be the reaction with OH and $O(^1D)$, resulting in several years atmospheric residence [*Cicerone and Zellner*, 1983]. However, this long lifetime cannot explain the variability of HCN observed with ground-based infrared solar spectroscopy in recent years [e.g., *Mahieu et al.*, 1995; *Rinsland et al.*, 1999; *Zhao et al.*, 2000]. A 2–4 month lifetime in the atmosphere was evaluated using a three-dimensional (3-D) chemical and transport model with biomass burning as the primary source and ocean uptake as the main sink [*Li et al.,* 2000]. However, the HCN lifetime is still under discussion.

[3] Since HCN is a relatively inactive species, it is assumed to be a potential tracer of biomass burning emission [e.g., *Rinsland et al.*, 2001]. Tropospheric CO and HCN amounts at the subtropical station of Mauna Loa Observatory (19.5°N, 155.6°W, 3.4 km asl) were enhanced in 1997, possibly because of biomass burning that occurred in southeast Asia [*Rinsland et al.*, 1999]. Additional production of HCN and CO above their seasonal mean levels over Rikubetsu (43.5°N, 143.8°E, 0.2 km asl) and Moshiri (44.4°N, 142.3°E, 0.2 km asl) in northern Japan during 1995–1997 has been attributed to the biomass burning on the Asian continent [*Zhao et al.*, 2000]. Simultaneous enhancements of HCN and CO were also observed at the International Scientific Station at Jungfraujoch (ISSJ) (46.6°N, 8.0°E, 3.6 km asl) in 1998 and might be also related to the Asian biomass burning [*Rinsland et al.*, 2000].

[4] Biomass burning has been observed to often occur in tropical regions during the dry season and can also happen throughout the year at midlatitudes, including the regions of Asian continent such as Mongolia and eastern Siberia. *Tanimoto et al.* [2000] reported high surface CO at Rishiri Island (45.1°N, 141.1°E, 0.04 km asl) in northern Japan in 1998 due to biomass burning in eastern Siberia. Mean wind streamline fields between 200–850 hPa indicate that northern Japan is located downwind of the Asian continent outflow throughout the year [*Bachmeier et al.*, 1996; *Merrill et al.*, 1997]. Therefore Rikubetsu and Moshiri are ideally located for the detection of emissions from biomass burning occurring on Asian continent. Previous measurements of HCN and CO at Moshiri and Rikubetsu in 1995–1997 showed simultaneous enhancements of HCN and CO from the Asian continental biomass burning [*Zhao et al.*, 2000]. This paper presents measurements of tropospheric CO, C_2H_6, C_2H_2, and HCN over northern Japan for the period from May 1995 to June 2000. Extension of the measurement period enabled more reliable characterization of the seasonal variations and the detection of trends in the concentrations of these species. The effects of the eastern Siberia fires in July–October 1998 were also observed in the extended data set.

2. Observations

[5] Measurements of atmospheric CO, C_2H_6, C_2H_2, and HCN using high spectral resolution ground-based Fourier transform infrared (FTIR) spectrometers started at Rikubetsu in May 1995 and at Moshiri in April 1996. The FTIR instrument at Rikubetsu was a Bruker IFS 120M with 257 cm of optical path difference (OPD) and that at Moshiri was a Bruker IFS 120HR with 450 cm of OPD. Defined as 0.9/OPD, the highest spectral resolution of the two instruments was 0.0035 and 0.0020 cm^{-1}, respectively. Each instrument was operated, for the present purpose, in the 2.7–5.0 μm spectral region with an InSb detector and three optical filters (2.70–3.57 μm, 3.13–4.17 μm, and 3.85–5.00 μm). The focal length (FL) of the Bruker 120M was 220 mm, and its entrance aperture (APT) diameters ranged from 0.50 to 0.85 mm, resulting in 2.27–3.86 mrad field of view (FOV). The corresponding FL, range of APT, and range of FOV of the Bruker 120HR were 418 mm, 0.80 to 1.30 mm, and 1.91 to 3.11 mrad, respectively.

[6] Since the absorption lines of tropospheric species are broadened by pressure, each line shape contains information on the absorption at different altitudes. The infrared solar spectra were usually measured at the maximum spectral resolution with boxcar apodization in order to record as much information as possible for the retrieval of the vertical mixing ratio profile. Sometimes, lower resolutions (0.007 cm^{-1} at Rikubetsu and 0.0035 cm^{-1} at Moshiri) were adopted to reduce the measurement time when weather conditions were marginal. In order to achieve a better signal-to-noise ratio (SNR), 2–8 interferograms were coadded to create a spectrum. Depending on both spectral resolution and the number of interferograms, it usually took 5–10 min to complete the measurement of a solar spectrum.

[7] The FTIR measurements at Moshiri were made routinely from April 1996, while those at Rikubetsu were performed in a campaign mode with intensive activities during the winter seasons from May 1995 to April 1999, at which time routine measurements began at Rikubetsu. Because the ground-based FTIR instruments use direct sunlight, measurements only can be performed on clear days. Usually, the rate of clear days over Rikubetsu is high in winter, while that over Moshiri is high in summer. As a result, the measurements at the two locations covered different periods with some overlap. In addition, since the two sites are located far from major cities and at similar latitudes (44° ± 0.5°N), observational results at the two sites were very similar [*Zhao et al.*, 2000]. Therefore data observed at the two sites were combined to produce a single data set. In total, there were 651, 723, 649, and 648 days for the measurements of CO, C_2H_6, C_2H_2, and HCN respectively between May 1995 and June 2000.

3. Data Analysis

3.1. Method

[8] The ground-based infrared solar spectra were analyzed using the SFIT2 algorithm, which was jointly developed at the NASA Langley Research Center and the

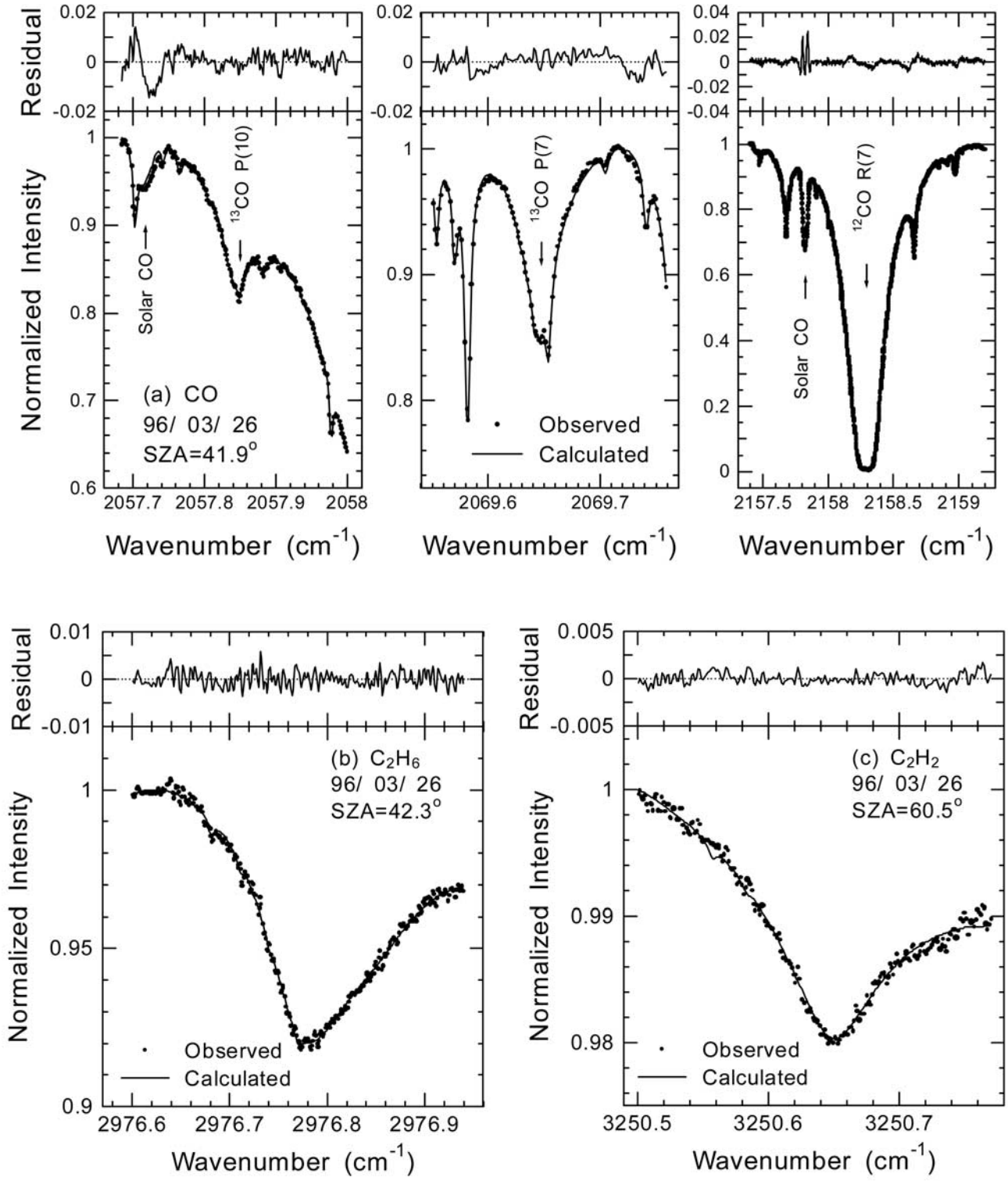

Figure 1. Microwindows of ground-based infrared solar spectra for (a) CO, (b) C_2H_6, (c) C_2H_2, and (d) HCN. Examples of observed spectra are presented with circles, calculated spectra (the best fits) are solid lines, and the residuals between the observed and calculated spectra are shown in the upper panels on expanded scales.

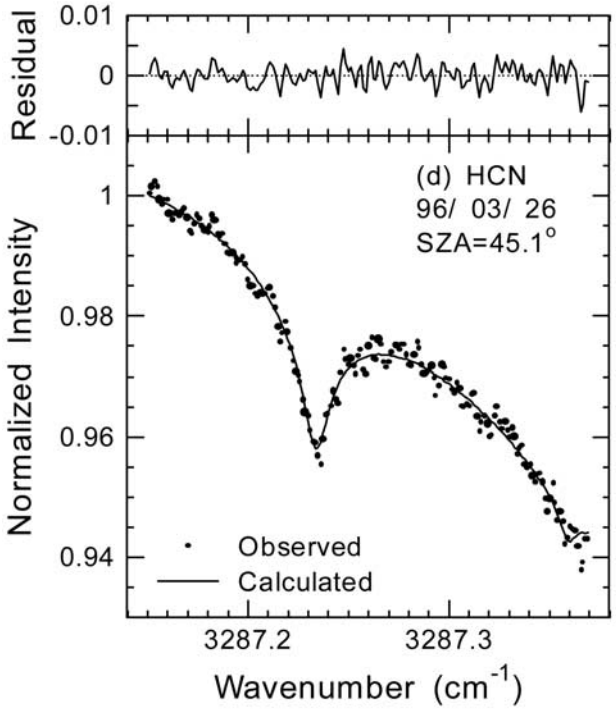

Figure 1. (continued)

National Institute of Water and Atmosphere Research at Lauder, New Zealand. This algorithm has been described in previous papers [e.g., *Pougatchev et al.*, 1995; *Rinsland et al.*, 1998, 1999, 2000]. Using this algorithm, the vertical mixing ratio profiles of one or two molecules can be retrieved by simultaneously fitting the absorption in one or more microwindows in one or more infrared solar spectra. Interfering absorption by other atmospheric molecules in the selected microwindows can be fitted simultaneously by scaling each of their a priori profiles. Solar CO lines can also be simulated in the SFIT2 algorithm to minimize the residuals of the spectral fitting [*Rinsland et al.*, 1998].

3.2. Spectral Intervals and Line Parameters

[9] Spectral intervals (microwindows) used to retrieve the atmospheric CO, C_2H_6, C_2H_2, and HCN mixing ratio profiles are shown in Figures 1a–1d and summarized in Table 1, along with a list of the interfering molecules in each window. These microwindows have been used previously by *Pougatchev and Rinsland* [1995], *Rinsland et al.* [1998, 1999, 2000] and *Notholt et al.* [2000] to retrieve total or partial column and mixing ratio profiles of atmospheric CO, C_2H_6, C_2H_2, and HCN from ground-based FTIR spectra.

[10] CO was retrieved by simultaneously fitting the spectra in three microwindows: 2057.68–2058.00 cm^{-1}, 2069.55–2069.76 cm^{-1}, and 2157.30–2159.15 cm^{-1}. These windows include a weak P(10) line of ^{13}CO at 2057.8578 cm^{-1}, a weak P(7) line of ^{13}CO at 2069.6559 cm^{-1}, and a strong R(7) line of ^{12}CO at 2158.2997 cm^{-1}. In addition to the interfering absorption by atmospheric CO_2, O_3, N_2O, and H_2O, solar CO lines appear in these microwindows.

[11] C_2H_6, C_2H_2, and HCN were all retrieved from single microwindows. The microwindow between 2976.60 and 2976.94 cm^{-1} contains a $^PQ_3$ subbranch of the C_2H_6 ν_7 band centered at 2976.8 cm^{-1}. Interfering absorptions in this microwindow are weak O_3 lines and wings of nearby H_2O and CH_4 lines. In the microwindow from 3250.50 to 3250.70 cm^{-1}, absorption of C_2H_2 at 3250.6633 cm^{-1} had been identified as the P(13) line of the $\nu_2 + \nu_4 + \nu_5$ band from Kitt Peak (31.9°N, 111.6°W, 2.1 km asl) solar absorption spectra [*Rinsland et al.*, 1985]. This line is located in the far wings of two $H_2{}^{16}O$ absorption lines and also close to weak absorption lines of $H_2{}^{17}O$ and $H_2{}^{18}O$. Since the abundance of atmospheric C_2H_2 is relatively low and absorption by C_2H_2 at 3250.6633 cm^{-1} is not very strong, C_2H_2 can only be quantitatively retrieved from ground-based solar spectra recorded at high solar zenith angle (SZA) or low-altitude sites. The intensity of the C_2H_2 absorption line at 776.0818 cm^{-1} is ~3 times stronger than that at 3250.6633 cm^{-1}. This line was used to retrieve C_2H_2 mixing ratio from Atmospheric Trace Molecule Spectroscopy (ATMOS) onboard the Spacelab 3 spectra [*Rinsland et al.*, 1987] and C_2H_2 columns from International Scientific Station of the Jungfraujoch (ISSJ) ground-based spectra [*Zander et al.*, 1991; *Mahieu et al.*, 1997]. Unfortunately, the C_2H_2 line at 776.0818 cm^{-1} could not be used in this study because of the nearby H_2O strong absorption, which is more serious at low-altitude sites and resulted in very low SNR for Rikubetsu and Moshiri solar spectra in this microwindow. There is a P(8) line of the HCN ν_3 fundamental band at 3287.2483 cm^{-1} in the microwindow from 3287.15 to 3287.37 cm^{-1}, which lies on the wing of a strong and broad H_2O line. The interference of nearby weak absorption lines of CO_2, O_3, and solar OH considered in our previous work [*Zhao et al.*, 2000] can be neglected by choosing a narrower spectral region that was used for this study.

[12] Spectral parameters for the atmospheric CO, C_2H_2, and HCN absorption lines were taken from the 1996 HITRAN compilation [*Rothman et al.*, 1998]. Updated spectral line parameters for C_2H_6 described by *Rinsland et al.* [1998] were used.

3.3. A Priori Profiles and Other Atmospheric Parameters

[13] The reference profiles of CO, C_2H_6, and C_2H_2 in the work of *Smith* [1982] were adopted as a priori profiles, with the tropospheric mixing ratios modified using in situ aircraft data obtained near Japan during the Pacific Exploratory

Table 1. Microwindows Used to Retrieve Tropospheric CO, C_2H_6, C_2H_2, and HCN

Molecule	Line Position, cm^{-1}	Spectral Region, cm^{-1}	Interfering Absorption
	2057.8578	2057.68–2058.00	CO_2, N_2O, O_3, solar CO
CO	2069.6559	2069.55–2069.76	CO_2, N_2O, O_3
	2158.2997	2157.30–2159.15	H_2O, N_2O, O_3, CO_2, solar CO
C_2H_6	2976.759[a]	2976.60–2976.94	H_2O, CH_4, O_3
C_2H_2	3250.6624	3250.50–3250.70	H_2O
HCN	3287.2483	3287.15–3287.37	H_2O

[a] Center of the absorption band.

Mission-West Phase A (PEM-West A) and PEM-West B experiments [*Talbot et al.*, 1996, 1997; *Blake et al.*, 1997]. Tropopause heights determined by Sapporo (43.1°N, 141.3°E) rawinsonde data were also taken into account in constructing the a priori profiles, owing to the rapid decrease in the mixing ratios of these molecules across the tropopause. For HCN the reference profile given by *Mahieu et al.* [1995] was used as the a priori profile, with a constant mixing ratio of 185 parts per trillion (pptv) below 10 km.

[14] Strong absorption by H_2O is present throughout the spectral region from 2.7 to 5.0 μm, which was used in this study. Because H_2O is an interfering gas in the microwindows used to retrieve the tropospheric CO, C_2H_6, C_2H_2, and HCN, selection of the a priori profiles of H_2O is very important for the accurate retrievals. Daily rawinsondes data obtained in Sapporo were used to create the tropospheric H_2O profile, while monthly zonal mean H_2O profiles at 40°–50°N measured by the Halogen Occultation Experiment (HALOE) onboard the Upper Atmosphere Research Satellite (UARS) were used for the stratospheric profiles. Daily a priori H_2O profiles were constructed by smoothly connecting the daily tropospheric values with the monthly mean stratospheric profiles. O_3 is another major interfering gas in the selected microwindows for CO and C_2H_6 (see Table 1). Monthly mean profiles of ozonesonde data obtained at Sapporo from 1980 to 1990 were chosen as the initial values of O_3. A priori mixing ratio profiles of other interfering molecules were taken from the reference compilation by *Smith* [1982].

[15] Covariances of the CO, C_2H_6, C_2H_2, and HCN mixing ratio vectors [e.g., *Rinsland et al.*, 1998] were assumed to be diagonal. The relative uncertainties of the a priori mixing ratio profiles for C_2H_6, C_2H_2, and HCN were assumed to be 0.75, 0.80, and 1.0, respectively, for all 29 layers in the atmospheric model. For CO the assumed values were 0.25 between 0.2 and 20 km, increased to 2 at 40 km, and remained 2 above 40 km.

[16] Daily pressure–temperature-altitude profiles were constructed using rawinsonde data obtained four times a day at Sapporo. Since the maximum altitude reached by the rawinsondes was usually less than 35 km, the profiles above that height were smoothly connected to the 1976 U.S. Standard Atmosphere.

3.4. Averaging Kernels

[17] The altitude sensitivity of the retrievals can be theoretically characterized using averaging kernels [e.g., *Rodgers*, 1990]. Averaging kernels at each altitude were calculated for the measurements of CO, C_2H_6, C_2H_2, and HCN using ground-based infrared solar spectroscopy. Because of the poor vertical resolution of infrared remote sensing methods, retrievals at all altitudes are not independent. Therefore only averaging kernels at some merged layers are representative [e.g., *Pougatchev et al.*, 1995]. Figure 2 shows averaging kernels for CO, C_2H_6, C_2H_2, and HCN at selected layers. According to the distribution of the averaging kernels, partial columns of C_2H_6, C_2H_2, and HCN can be retrieved in two thick layers of 0.2–12 and 12–100 km, while partial columns of CO can be retrieved in three layers of 0.2–4, 4–12, and 12–100 km since the averaging kernels for these three layers have maximum values in the representative altitude regions. In most cases, CO columns in the broad layer between 0.2 and 12 km are presented in this paper to compare with C_2H_6, C_2H_2, and HCN results at the same altitude region. For comparison with surface CO measurements, CO mixing ratios retrieved between 0.2 and 4 km were used. It is seen from Figure 2 that averaging kernels of each molecule at different layers overlap, indicating that retrievals at the selected thick layers are still not totally independent. The layer between 0.2 and 12 km corresponds roughly to the troposphere over northern Japan, as the tropopause height determined by Sapporo rawinsonde data ranges from 8 km in winter to 16 km in summer. Therefore the retrievals in the 0.2–12 km layer represent the tropospheric partial columns of CO, C_2H_6, C_2H_2, and HCN. A contribution from the altitudes above 12 km to the 0.2–12 km retrieval, due to the overlapping of the averaging kernels, is small because of the relatively low stratospheric columns of the four molecules. Ratios of the column amounts above 12 km to the column amounts below 12 km are less than 10, 7, 1, and 20% for CO, C_2H_6, C_2H_2, and HCN, respectively.

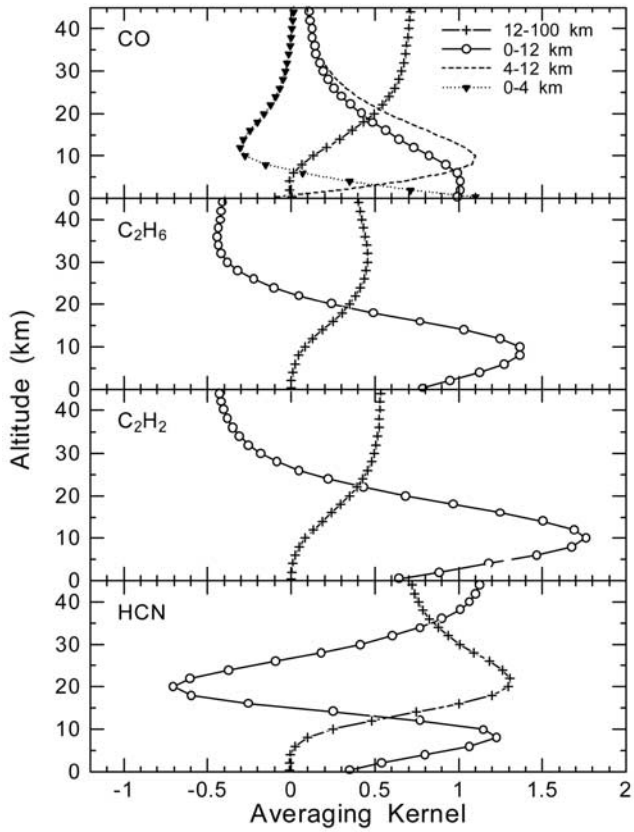

Figure 2. Averaging kernels calculated for CO, C_2H_6, C_2H_2, and HCN retrievals from ground-based infrared solar spectra obtained in northern Japan.

3.5. Error Budgets

[18] Error budgets for SFIT2 retrievals have been discussed by *Rinsland et al.* [1998, 1999, 2000]. Similar budgets were considered in this study and the results are summarized in Table 2.

Table 2. Error Budgets for the Retrievals of Tropospheric CO, C_2H_2, C_2H_6, and HCN[a]

Error Sources	CO	C_2H_6	C_2H_2	HCN
Forward model approximation	4	2	2	2
Spectroscopic parameters	2	5	10	2
Instrumental line shape	1.2	<1	<1	1.6
A priori profile	1.5	4.1	9.7	15
Total systematic errors	4.9	6.8	14.0	15.3
RMS noise	<1	2.2	13	7.4
SZA	<1	<1	<1	<1
Temperature	4.2	4.3	1.0	3.2
Interference	<1	<1	4.0	<1
Total random errors	4.5	5.0	13.7	8.2

[a] Error budgets are in percent. Columns between 0.2 and 12 km.

[19] Errors caused by the forward model simulation of solar absorption spectra and by the spectroscopic parameters for CO, C_2H_6, and HCN are the same as those given in the papers cited above, because the same retrieval algorithm and spectral parameters were employed. For C_2H_2 the error due to the forward model approximation was assumed to be the same as that for C_2H_6. The C_2H_2 spectroscopic parameters at P(13) line of the $\nu_2 + \nu_4 + \nu_5$ band were interpolated from its R(9) line of the $\nu_4 + \nu_5$ band [*Rinsland et al.*, 1985]. As a rough estimate, the error due to the uncertainty in C_2H_2 spectroscopic parameters was 10%, twice that for C_2H_6.

[20] Errors due to instrumental line shape, a priori profiles, altitude-pressure-temperature profiles, random spectral noise, and interference by H_2O absorption are different from those estimated in the papers cited above due to the different locations and FTIR instruments used for the measurements. Therefore these error budgets were analyzed using synthetic spectra.

[21] The FTIR instrumental line shape is simulated in the SFIT2 algorithm using an effective appodization function and an effective phase function. As an approximation, the effective appodization function is expressed as an empirical polynomial, representing the modulation of the interferogram signal. Assuming 50% uncertainty in the coefficient of the straight line of the effective appodization function resulted in 1.0–1.5% errors, indicating that the retrieved tropospheric partial columns were almost insensitive to the instrument line shape for the four molecules.

[22] Errors due to the a priori profile were evaluated using synthetic spectra. First, the original a priori profile was modified by adding a spike at every 2 km layers, in which the mixing ratio was increased by 100%. This is to simulate the cases that real mixing ratio profiles are not very smooth. Columns corresponding to these modified profiles are called "true." Then, a set of synthetic spectra were generated using these modified profiles and were analyzed using the original a priori profile with the SFIT2 method (the resulting columns are called "retrieved"). The difference between true and retrieved columns for each synthetic spectrum is resulted from the spike in the mixing ratio profile at every 2 km. The sum of the differences at all layers in the troposphere are 1.5, 4.1, 9.7, and 15% for CO, C_2H_2, C_2H_6, and HCN, respectively.

[23] On the basis of the typical noise level for CO, C_2H_6, C_2H_2, and HCN spectra recorded in northern Japan, 1% random noise was added to the synthetic CO spectra and 0.3% random noise was added to the C_2H_6, C_2H_2, and HCN spectra. The resulting errors in the partial columns between 0.2 and 12 km were <1, 2.2, 13, and 7.4% for CO, C_2H_6, C_2H_2, and HCN, respectively. A solar spectrum was usually recorded in 5–10 min, which corresponds to a 2% change in SZA during sunrise and sunset in northern Japan and hence induces an error in airmass calculations for each spectrum. The resulting errors in the retrieved partial columns were found to be less than 1%. Since the altitude-pressure-temperature profiles were constructed using daily rawinsonde data obtained at Sapporo, they should be close to the values at Rikubetsu and Moshiri. Assuming ±5°C accuracy in temperature profiles, errors of 4.2, 4.3, 1.0, and 3.2% were obtained for CO, C_2H_6, C_2H_2, and HCN partial columns, respectively. In order to account for errors introduced by the interfering H_2O absorption in the selected microwindows, 50% uncertainty was assumed in the daily Sapporo rawinsonde data for H_2O mixing ratios between 0.2 and 4 km. This resulted in errors of 4.0% for C_2H_2 and less than 1% for CO, C_2H_6, and HCN retrievals.

[24] Total estimated errors for the retrievals of tropospheric CO, C_2H_6, C_2H_2, and HCN columns between 0.2 and 12 km are 6.7, 8.4, 19.6, and 17.5%, respectively.

3.6. Spectra and Fits

[25] Figures 1a–1d display typical ground-based infrared solar spectra of CO, C_2H_6, C_2H_2, and HCN in the microwindows listed in Table 1, together with their fits and the RMS residuals between the observed and calculated spectra. These spectra were observed at Rikubetsu on March 26, 1996, with resolution of 0.0035 cm^{-1}. The SZA for the CO, C_2H_6, C_2H_2, and HCN spectra was 41.9°, 42.3°, 60.5°, and 60.5°, respectively. The FOV was 2.95, 2.27, 2.27, and 2.27 mrad. The SNR for the CO spectrum in Figure 1a was 287 near 2158.30 cm^{-1}, which was a typical SNR value for CO spectra throughout the year. The SNR for the C_2H_6, C_2H_2, and HCN spectra in Figures 1b–1d was 40, 13, and 14, respectively. Generally, the SNR ranged from 5 to 150, 2 to 40, and 4 to 80 for the C_2H_6, C_2H_2, and HCN spectra, respectively, with higher SNR values in winter-spring because C_2H_6 and C_2H_2 column amounts were high in these seasons. Although HCN amounts increase in summer-fall [*Zhao et al.*, 2000], the SNR for the HCN spectra was low in these seasons because of the increase in H_2O, which is a major interfering gas. The maximum RMS residuals were 1% for the CO spectral fits. As can be seen in Figure 1a, greater residuals mainly appear in the spectral regions of solar CO lines owing to uncertainty in modeling these solar CO lines. Therefore the residuals in these spectral regions were de-weighted for the convergence test in the SFIT2 optimal estimation subroutine. The maximum RMS residuals for the C_2H_6, C_2H_2, and HCN spectral fits were all 0.3%. The minimum SNR and maximum RMS values discussed above were used to check data quality, i.e., results from spectra with either the SNR lower than the minimum values or the RMS residuals higher than the maximum values are excluded in this paper.

4. Results and Discussion

4.1. Seasonal Cycles

[26] Daily averages of the tropospheric (0.2–12 km) column amounts and mixing ratios of CO, C_2H_6, C_2H_2,

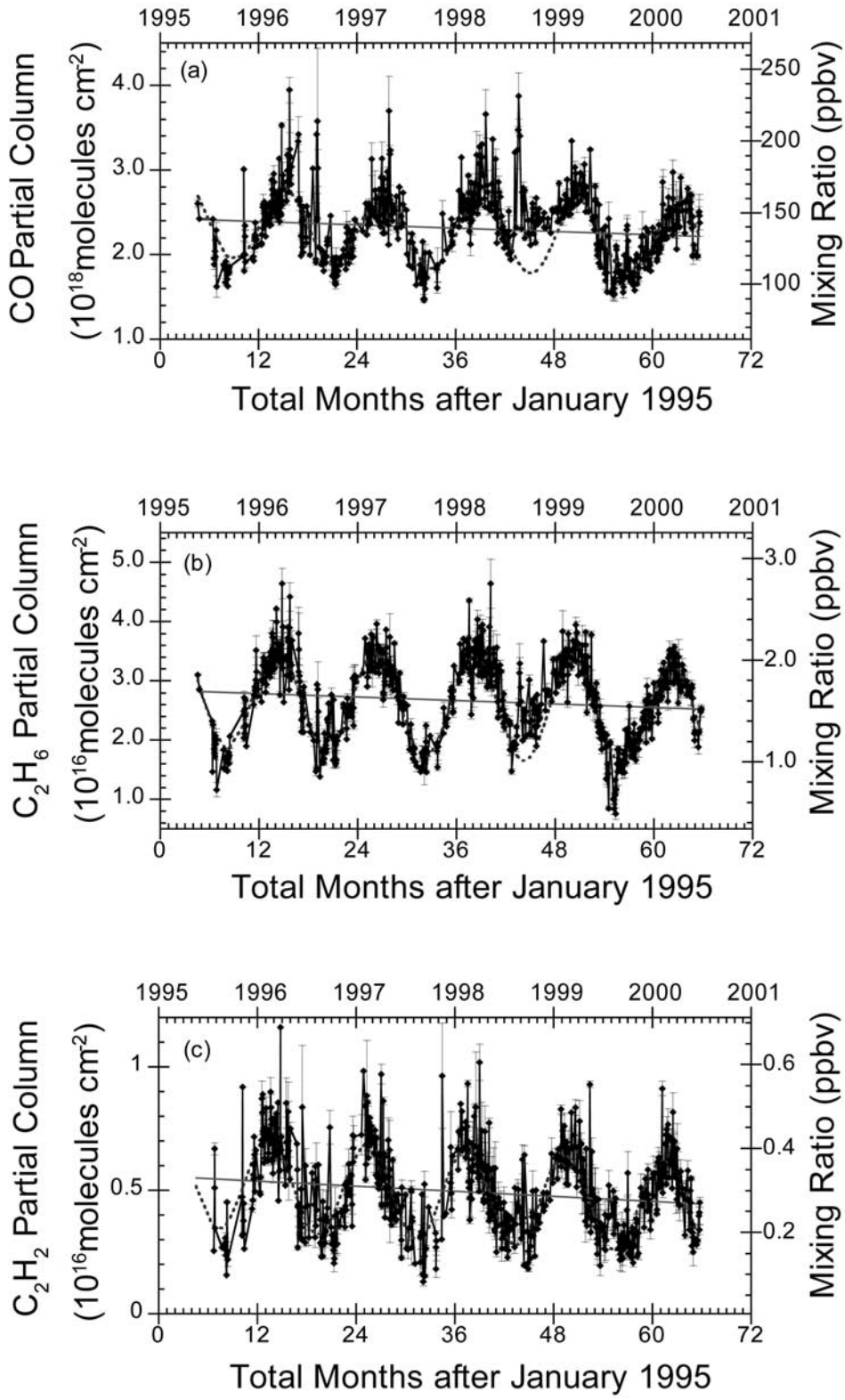

Figure 3. Daily averages of the tropospheric columns and mixing ratios between 0.2 and 12 km of (a) CO, (b) C_2H_6, (c) C_2H_2, and (d) HCN over northern Japan. Vertical error bars represent one standard deviation ($\pm\sigma$) in the daily mean values. Data without error bars mean a single measurement on that day. Cosine curves are the least squares best fits to the daily values between May 1995 and June 2000 (excluding the 1998 period) using equation (1). Straight lines are linear trends of the four molecules determined from the ratio of c_1 to c_0 in equation (1).

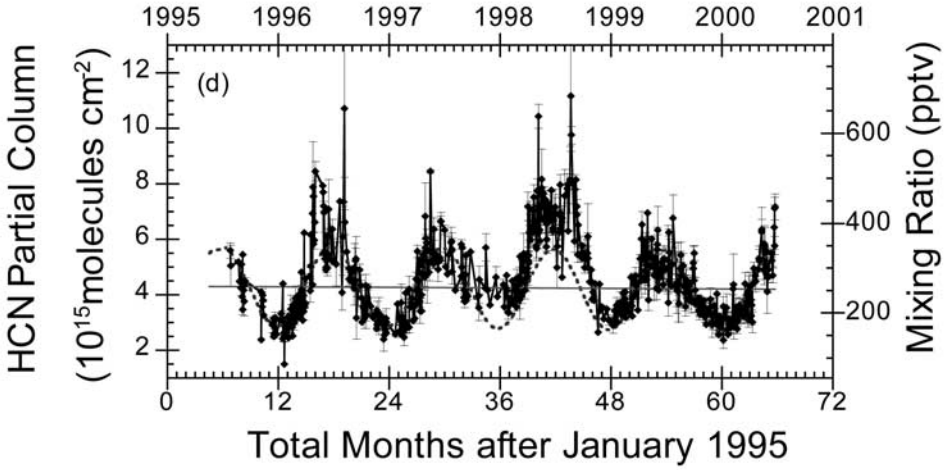

Figure 3. (continued)

and HCN observed in northern Japan from May 1995 to June 2000 are shown in Figures 3a–3d. The mixing ratios were determined by dividing the partial column between 0.2 and 12 km by the total air column at the same layer. Vertical bars in Figures 3a–3d represent one standard deviation (SD) in the daily mean values. Data with no error bar are measurements from a single spectrum in one day. The SD in the daily partial column was usually less than 15% for CO and C_2H_6, less than 30% for C_2H_2, and less than 25% for HCN. However, some high SD values were obtained on a number of days, resulting from strong diurnal variability on these days. These large SD values were obtained simultaneously for CO, C_2H_6, C_2H_2, and HCN and enhancements in the four molecules were also observed on the same days.

[27] Significant seasonal variations in the tropospheric columns and mixing ratios of CO, C_2H_6, C_2H_2, and HCN are readily seen in Figures 3a–3d. Cosine curves in the figures represent the background levels of the seasonal mean for each molecule. These were derived from the least squares best fits to the daily partial columns from May 1995 to June 2000 using the formula:

$$\text{partial column} = c_0 + c_1 t + c_2 \cos[(2\pi/12)(t - \phi_0)] \quad (1)$$

where t expresses time in months elapsed since January 1995. Coefficients of c_0, c_1, c_2, and ϕ_0 represent the annual mean value of the partial column in 1995, the linear change in the partial column, the amplitude of the seasonal modulation, and the phase of the seasonal cycle, respectively. Since remarkably high CO, C_2H_6, C_2H_2, and HCN were observed in 1998, the 1998 data were excluded from the least squares fits using equation (1). Table 3 summarizes the seasonal variations of CO, C_2H_6, C_2H_2, and HCN in northern Japan and compares the results with in situ aircraft measurements at ~45°N over the west Pacific region during PEM–West B (February–March 1994) [*Singh et al.*, 1998].

4.1.1. Carbon Monoxide (CO)

[28] The CO partial columns between 0.2 and 12 km reached a maximum level of $2.70 \pm 0.31 \times 10^{18}$ molecules cm^{-2} in winter-spring (March–April) and a minimum level of $1.83 \pm 0.19 \times 10^{18}$ molecules cm^{-2} in fall (September–October). Maximum and minimum CO mixing ratios in the same layer were found to be 162 ± 21 ppbv and 111 ± 13 ppbv, respectively. The seasonal cycle of CO is primarily driven by the reaction with OH whose concentration in summer-fall is greater than that in winter-spring [e.g., *Volz et al.*, 1981]. In addition, some CO sources, such as biomass

Table 3. Seasonal Variations in Tropospheric CO, C_2H_6, C_2H_2, and HCN Over Northern Japan

	Maximum Values[a]			PEM-West B[b] (February–March 1994)		Minimum Values		
	Month	Column Amount	Mixing Ratio	Mixing Ratio	Altitude, km	Month	Column Amount	Mixing Ratio
CO	March–April	2.70 ± 0.31	162 ± 21	130 180 180	6–12 3–7 0–3	Sept.–Oct.	1.83 ± 0.19	111 ± 13
C_2H_6	Feb.–March	3.36 ± 0.30	2.00 ± 0.18	1.50 2.30 2.30	6–12 3–7 0–3	Aug.–Sept.	1.76 ± 0.40	1.07 ± 0.25
C_2H_2	Feb.–March	0.67 ± 0.10	0.40 ± 0.07	0.40 0.75 0.75	6–12 3–7 0–3	Sept.–Oct.	0.30 ± 0.10	0.19 ± 0.06
HCN	May–July	5.50 ± 0.91	334 ± 30	...	...	Dec.–Jan.	3.02 ± 0.49	179 ± 30

[a] Column amounts for CO, C_2H_6, C_2H_2, and HCN are in 10^{18}, 10^{16}, 10^{16}, and 10^{15} molecules cm^{-2}, respectively, and mixing ratios are in ppbv, ppbv, ppbv, and pptv.

[b] From *Singh et al.* [1998].

burning and fossil fuel usage, are usually enhanced in the dry and cold conditions of winter-spring, resulting in greater CO production in this period [*Zhao et al.*, 1997].

4.1.2. Ethane (C_2H_6)

[29] The maximum C_2H_6 partial column was $3.36 \pm 0.30 \times 10^{16}$ molecules cm^{-2} in winter-spring (February–March) and the minimum was $1.76 \pm 0.40 \times 10^{16}$ molecules cm^{-2} in summer-fall (August–September). The corresponding maximum and minimum C_2H_6 mixing ratios were 2.00 ± 0.18 and 1.07 ± 0.25 ppbv, respectively. The C_2H_6 seasonal cycle is mainly controlled by the balance between its sources (biomass burning and natural gas emissions) and its sink (chemical reaction with OH) [*Rinsland et al.*, 2000, and references therein]. According to the phases (ϕ_0) fitted using equation (1), C_2H_6 reached its maximum level in winter-spring ~1 month earlier than CO did, partly because CO is an intermediate product of the oxidation of CH_4 and NMHCs, while C_2H_6 is the most abundant of the NMHCs [*Volz et al.*, 1981; *Logan et al.*, 1981].

4.1.3. Acetylene (C_2H_2)

[30] The C_2H_2 partial column reached a maximum of $0.67 \pm 0.10 \times 10^{16}$ molecules cm^{-2} in February–March and a minimum of $0.30 \pm 0.10 \times 10^{16}$ molecules cm^{-2} in September–October. The maximum and minimum C_2H_2 mixing ratios were 0.40 ± 0.07 and 0.19 ± 0.06 ppbv, respectively. As NMHCs, C_2H_2 and C_2H_6 have similar sources and sinks. Therefore the dynamics of the C_2H_2 seasonal cycle is similar to that for C_2H_6. The phase, ϕ_0 in equation (1), of the C_2H_2 seasonal cycle is about a half month ahead of C_2H_6, possibly because that the photochemical reaction rate of C_2H_2 with OH is faster than that of C_2H_6 with OH [*Logan et al.*, 1981; *Singh and Zimmerman*, 1992].

4.1.4. Hydrogen Cyanide (HCN)

[31] The HCN partial column reached a maximum of $5.50 \pm 0.91 \times 10^{15}$ molecules cm^{-2} in May–July and a minimum of $3.02 \pm 0.49 \times 10^{15}$ molecules cm^{-2} in December–January. The maximum and minimum values of the tropospheric HCN mixing ratio were 334 ± 50 and 179 ± 30 pptv, respectively, which are consistent with our previous results derived from 1995–1997 data [*Zhao et al.*, 2000]. The HCN seasonal cycle over northern Japan between 1995 and1997 was roughly simulated by a 3-D chemical and transport model using tropical biomass burning as a primary source and ocean uptake as a main sink [*Li et al.*, 2000]. Biomass burning on Asian continent could also contribute to the enhanced HCN values above its seasonal background level over northern Japan [*Zhao et al.*, 2000].

[32] In Table 3 it can be seen that tropospheric mixing ratios of CO and C_2H_6 retrieved from ground-based FTIR spectra agreed well with the in situ aircraft measurements at 45°N over the west Pacific region during PEM-West B (February–March 1994) [*Singh et al.*, 1998]. However, the retrieved mixing ratios of C_2H_2 were lower than the aircraft data. Comparison with in situ aircraft measurements revealed that the tropospheric mixing ratios retrieved from the ground-based FTIR spectra are a smoothed representation of the real vertical distributions [*Zhao et al.*, 1997], as expected from the averaging kernel calculations.

4.2. Correlations

[33] It can be seen in Figures 3a–3c that the tropospheric CO, C_2H_6, and C_2H_2 columns reached their maximum and minimum values in similar seasons. Simultaneous enhancements in tropospheric CO, C_2H_6, and C_2H_2 indicate the same sources of polluted air. These features reveal that changes in tropospheric concentrations of the three molecules are correlated.

[34] Figures 4a–4c are correlation plots between the daily mean values of the tropospheric CO, C_2H_6, and C_2H_2 columns. The correlation coefficients of 0.80 between C_2H_6 and CO, 0.67 between C_2H_2 and CO, and 0.81 between C_2H_2 and C_2H_6 were obtained by linear least squares fits to the data from all seasons. The good correlations indicate that the three molecules are subject to similar production and dilution processes. The correlation coefficient between CO and C_2H_2 was relatively low, partly because their phases of the seasonal cycle were about one and half months different resulting from the discrepancies between their sources and sinks. For instance, the photochemical lifetime is ~1 month for C_2H_2 and ~2 months for CO [*Logan et al.*, 1981; *Volz et al.*, 1981; *Gupta et. al.*, 1998]. However, some low C_2H_6 values observed in summer 1998 (see Figure 3b) do not seem to be correlated with CO (see Figure 4a). The causes of this are not yet understood.

[35] Good correlations between tropospheric C_2H_6 and CO have been observed in other ground-based FTIR measurements at Lauder, Kitt Peak [*Rinsland et al.*, 1998], Mauna Loa [*Rinsland et al.*, 1999], and ISSJ [*Rinsland et al.*, 2000]. The slope of 13.2×10^{-3} for the C_2H_6 versus CO plot obtained in northern Japan agrees well with northern midlatitude observations at Kitt Peak (14.2×10^{-3}) [*Rinsland et al.*, 1998] and ISSJ (12.9×10^{-3}) [*Rinsland et al.*, 2000]. Aircraft measurements at 25°–48°N over the west Pacific region during PEM-West B produced a C_2H_6/CO slope of 15.0×10^{-3} for nonplume data above 2 km [*Blake et al.*, 1997].

[36] The slope for the C_2H_2 versus CO plot observed in northern Japan was 2.85×10^{-3}. According to our knowledge, the C_2H_2/CO slope had not been reported previously from ground-based FTIR measurements. Therefore we do not have an opportunity to compare with other ground-based data sets. However, a C_2H_2/CO slope of 5.7×10^{-3} was obtained in in situ aircraft measurements at 25°–48°N over the west Pacific region during PEM-West B [*Blake et al.*, 1997], which was twice the value of this work. Since the PEM-West B data covered a wide range of latitudes, while the FTIR measurements were made at 43.5°N and 44.4°N, latitudinal changes in tropospheric CO and C_2H_2 mixing ratios could be a reason for this difference [*Singh et al.*, 1998; *Blake et al.*, 1997].

[37] It is seen from Figures 3a and 3d that the phases of the CO and HCN seasonal cycles were ~3–4 months different, apparently owing to differences in their sources and sinks. On the other hand, simultaneous significant enhancements in tropospheric CO and HCN were occasionally observed, possibly due to the similar sources. In order to remove the components of the seasonal cycle, the deviation of HCN (ΔHCN) relative to its seasonal mean determined with equation (1) was plotted against the similar deviation of CO (ΔCO), as shown in Figure 5. Red circles represent the 1998 data and black crosses represent all other data. The correlation coefficients of 0.68 for 1998 and 0.71 for the other years indicate a good correlation between

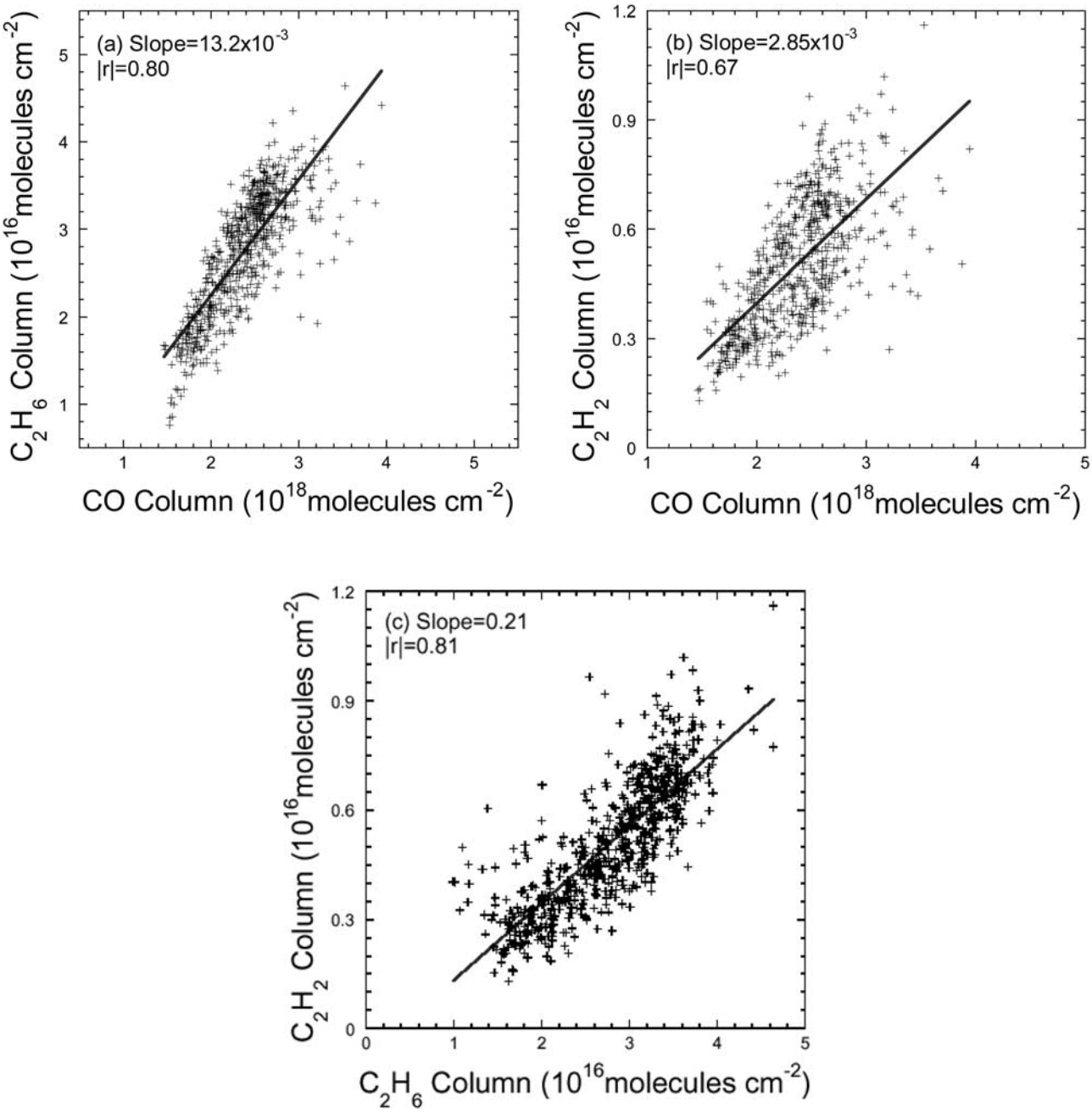

Figure 4. Correlation plots (a) between C_2H_6 and CO, (b) between C_2H_2 and CO, and (c) between C_2H_2 and C_2H_6. The data are daily averages of the tropospheric column amounts in the 0.2–12 km layer and from all seasons between May 1995 and June 2000.

ΔHCN and ΔCO, revealing that additional HCN and CO above their seasonal mean values were produced simultaneously.

[38] Laboratory and field fire studies reveal that both HCN and CO are emitted by biomass burning [*Yokelson et al.*, 1996, 1997; *Holzinger et al.*, 1999]. The emission ratio of HCN relative to CO in biomass burning varies by 2 orders of magnitude, depending on fire type, burnt biomaterials, and the phase of the fire [*Yokelson et al.*, 1996, 1997; *Holzinger et al.*, 1999]. In addition, this ratio also changes as the emitted air parcels undergo transport because CO and HCN have different atmospheric lifetimes. Therefore it is hard to establish a relationship between the HCN/CO emission ratio originating at the location of the fire and the HCN/CO ratio observed at a distant observational site. However, the ΔHCN/ΔCO slopes of 1.60×10^{-3} in 1998 and 2.02×10^{-3} in the other years observed in northern Japan lie between the wide range of values of the HCN/CO emission ratios measured in laboratory (0.4×10^{-3}–7.1×10^{-3} in the work of *Yokelson et al.* [1997] and $0.4 \times$

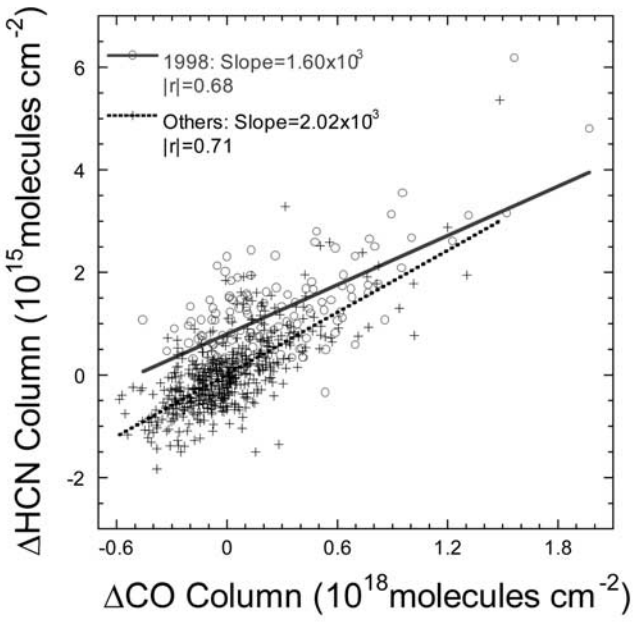

Figure 5. Correlation between ΔHCN and ΔCO. See text for details. See color version of this figure at back of this issue.

10^{-3}–2.6×10^{-3} in the work of *Holzinger et al.* [1999]). It is likely that the enhancement of HCN and CO above their seasonal mean values was due to biomass burning.

4.3. Linear Trend

[39] The linear trend in the partial column was determined by the ratio of c_1/c_0 in equation (1). The straight lines in Figures 3a–3d represent the linear trends in tropospheric column amounts of CO, C_2H_6, C_2H_2, and HCN from May 1995 to June 2000 over northern Japan. The 1998 data were excluded in determining the trends because abnormally high values were observed in this year.

[40] The annual mean tropospheric CO column amount over northern Japan in 1995 determined using equation (1) was 2.40×10^{18} molecules cm^{-2}. A linear trend of (-2.10 ± 0.30)%/yr in the CO partial column was obtained. In comparison, the observed trends in the CO partial column from May 1977 to December 1997 at Kitt Peak and in the CO total column during 1984–1995 at ISSJ were not significant. They were (-0.27 ± 0.17)%/yr [*Rinsland et al.*, 1998] and (0.18 ± 0.16)%/yr [*Mahieu et al.*, 1997], respectively. Network surface CO sampling measurements from 1990 to 1998 have also revealed a negative trend of −3%/yr in the southern hemisphere and −2%/yr in the northern hemisphere [*Novelli et al.*, 1998].

[41] The annual mean tropospheric C_2H_6 column amount over northern Japan was 2.77×10^{16} molecules cm^{-2} in 1995 with a negative linear trend of (-2.53 ± 0.30)%/yr. Ground-based infrared measurements at ISSJ from 1985 to 1995 indicated a decrease in the C_2H_6 total column with a rate of (-2.7 ± 0.3)%/yr [*Mahieu et al.*, 1997]. Trends in C_2H_6 at Lauder from 1993 to 1998 and at Kitt Peak from 1977 to 1997 were (-0.64 ± 0.79)%/yr and (-1.20 ± 0.35)%/yr, respectively [*Rinsland et al.*, 1998].

[42] The annual mean tropospheric C_2H_2 column amount over northern Japan was 0.54×10^{16} molecules cm^{-2} in 1995, indicating that the tropospheric abundance of C_2H_2 is ~20% that of C_2H_6. A negative linear trend of (-3.99 ± 0.57)%/yr was obtained for May 1995 to June 2000. This trend is larger than those obtained for C_2H_6 and CO. For comparison, the C_2H_2 trend of (-0.73 ± 1.15)%/yr observed at ISSJ from 1986 to 1995 was not significant [*Mahieu et al.*, 1997].

[43] The annual mean tropospheric HCN column amount over northern Japan was 4.34×10^{15} molecules cm^{-2} in 1995, corresponding to a tropospheric mixing ratio of 261 pptv. A negative linear trend of (-0.93 ± 0.49)%/yr in the HCN partial columns from May 1995 to June 2000 was obtained. This trend is very small and is generally consistent with the observations at ISSJ from 1995 to 1999 (excluding 1998 data) [*Rinsland et al.*, 2000] and at Kitt Peak from 1978 to 2000 [*Rinsland et al.*, 2001], where no significant long-term changes have been detected. In contrast, HCN measurements at ISSJ during 1984–1995 indicated an increase of $(1.24 \pm 0.0.36)$%/yr [*Mahieu et al.*, 1997].

[44] As stratospheric O_3 absorbs solar UV radiation, the depletion of global stratospheric O_3 since the mid-1980s has resulted in an increase in the amounts of solar UV radiation reaching the Earth's surface. A significant positive trend in the 305 and 340 nm irradiance was observed between January 1992 and December 1998 in Santiago (33.5°S), Chile [*Cabrera and Fuenzalida*, 1999]. Increases in UV-B radiation were also observed in various parts of Europe in 1990s [*Taalas et al.*, 2000, and references therein]. It appears that the observed negative trends in tropospheric CO, C_2H_6, and C_2H_2 over northern Japan are due to the increase in solar UV radiation through the photochemical reactions with OH. In addition to the increase in solar UV radiation, negative trend in the global surface CO between 1990 and 1998 was suggested partly because of the reduced emissions from biomass burning and anthropogenic sources in the past decade [*Novelli, et al.*, 1998]. This would also contribute to the negative trends in tropospheric CO, C_2H_6, and C_2H_2 over northern Japan.

4.4. Enhancements in 1998

[45] Remarkable enhancements of the tropospheric CO, C_2H_6, C_2H_2, and HCN concentrations were observed in

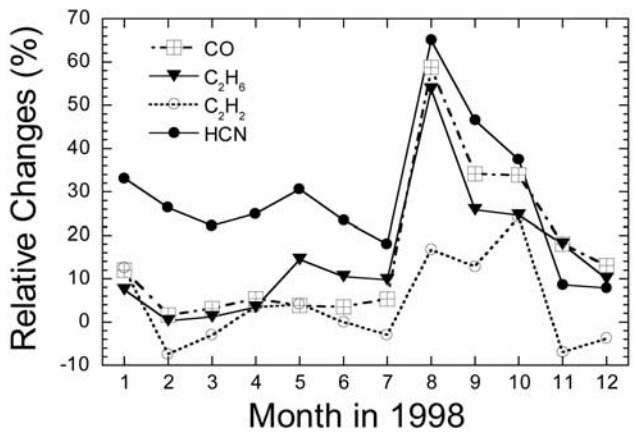

Figure 6. Changes in the tropospheric column amounts of CO, C_2H_6, C_2H_2, and HCN in 1998 relative to their seasonal mean values determined using equation (1).

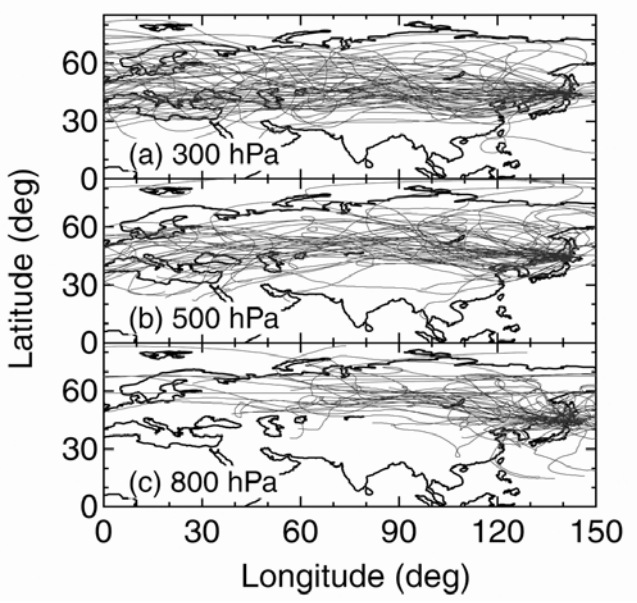

Figure 7. Kinematic 10-day back-trajectories calculated for the air masses reaching the (a) 300 hPa, (b) 500 hPa, and (c) 800 hPa levels over northern Japan. See color version of this figure at back of this issue.

1998. Changes in the tropospheric CO, C_2H_6, C_2H_2, and HCN column amounts relative to their seasonal mean values are shown in Figure 6. It can be seen that significant increases occurred between August and October 1998. The maximum increases in CO, C_2H_6, and HCN were 59, 54, and 65%, respectively, in August. By contrast, the relative change in tropospheric C_2H_2 was smaller than other molecules, with a maximum value of 22% in October. HCN columns were also elevated above the seasonal mean values by more than 20% from January to June 1998.

[46] Kinematic 10-day back-trajectories of the airmasses reaching the 300, 500, and 800 hPa levels above Rikubetsu and Moshiri were calculated for the days of FTIR measurements. For clarity, only trajectories from February, April, June, August, October, and December between 1997 and 1998 are plotted in Figure 7. It is seen that airmasses above 800 hPa level in northern Japan were mostly transported from the Asian and European continents at latitudes >30°N for all seasons. The calculated trajectories in other months and years exhibit the same results (not shown in Figure 7). Mean wind streamline fields averaged over the PEM-West A period (September–October 1991) [*Bachmeier et al.*, 1996] and the PEM-West B period (February–March 1994) [*Merrill et al.*, 1997] demonstrated similar behavior, indicating that northern Japan is downwind of the outflow of Asian continental air.

[47] Monthly global fire maps from 1995 to 2000 generated using ATSR-2 (Along Track Scanning Radiometer onboard the ERS-2 satellite) nighttime data in the ATSR World Fire Atlas (http://shark1.esrin.esa.it/FIRE/AF/ATSR/) [*Arino et al.*, 2001, and reference therein] show that fires were often observed over the Asian and European continents. It appears that biomass burning occurring there is an important source of tropospheric CO, C_2H_6, C_2H_2, and HCN observed in northern Japan. In addition to the fire maps, information on timing and location of the detected fires is available in the ATSR World Fire Atlas, from which the numbers of fires that occurred on the Asian and European continents in each month were accumulated. Figure 8 displays the number of fires observed in 1997 and 1998. "Region 1" covers the area from 90° to 150°E and above 30°N, roughly representing the Asian continent, and "Region 2" covers 0–90°E and above 30°N, representing the European and part of Asian continents. Since the data for other years in the ATSR World Fire Atlas are incomplete, they are not presented in Figure 8. For both 1997 and 1998 it is seen that the number of fires increased in the

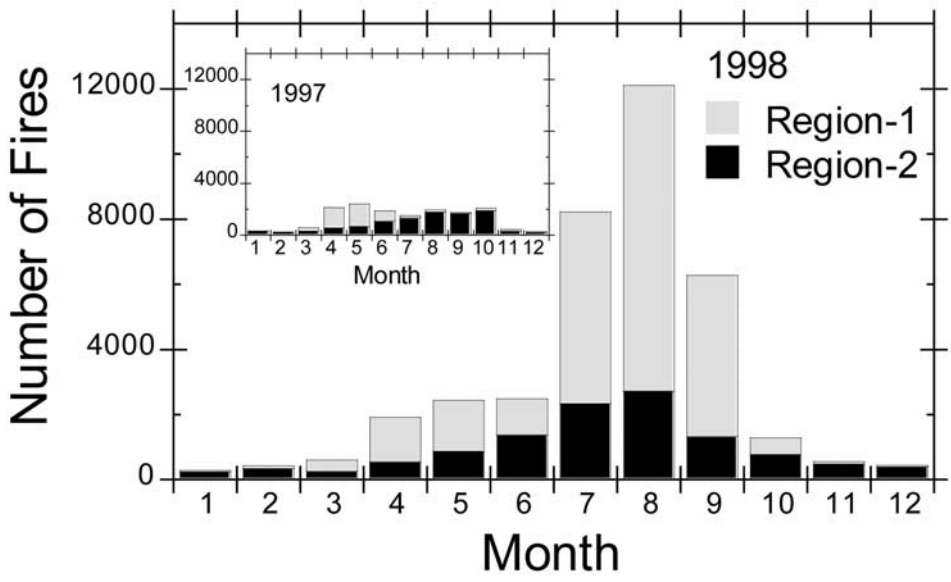

Figure 8. Number of fires in each month of 1997 and 1998 accumulated from the ATSR World Fire Atlas data. "Region-1" covers the area from 90 to 150°E and above 30°N and "Region-2" covers the area of 0-90°E and above 30°N.

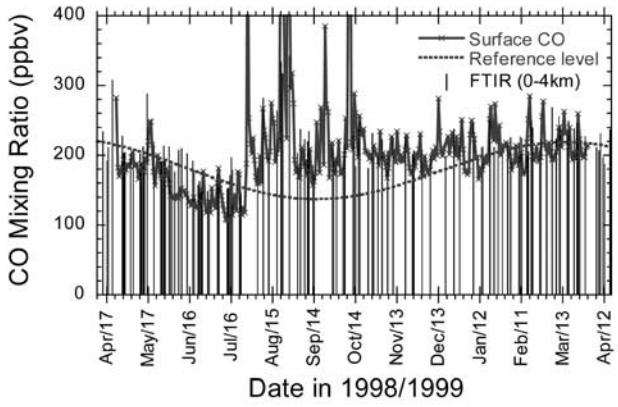

Figure 9. CO mixing ratios between 0.2 and 4 km over northern Japan from April 1998 to April 1999 retrieved from ground-based infrared solar spectra. Surface CO mixing ratios observed at Rishiri, Japan [*Tanimoto et al.*, 2000], are also shown for comparison. The dashed line represents the reference level of the seasonal mean 0.2–4 km CO mixing ratio derived from the best fit to the May 1995 to June 2000 data (excluding the 1998 period) using equation (1). See color version of this figure at back of this issue.

summer-fall season, acting as a source of HCN over northern Japan during this period [*Zhao et al.*, 2000]. It is also seen that the number of fires in 1998 was greatly enhanced in comparison with 1997, particularly on the Asian continent during July–September. The ATSR World Fire Atlas reveals that number of fires increased significantly over eastern Siberia near northern Japan around July–September 1998 (see http://shark1.esrin.esa.it/FIRE/AF/ATSR). Therefore it is most likely that these eastern Siberia fires were the cause of the significant enhancements of tropospheric CO, C_2H_6, C_2H_2, and HCN that were measured in northern Japan in those months.

[48] *Tanimoto et al.* [2000] reported high surface CO concentrations at Rishiri Island in northern Japan in 1998 due to the biomass burning in eastern Siberia. Since Rishiri is located not far away from Moshiri and Rikubetsu, the FTIR CO data from this work were compared with these surface CO measurements. As can be seen in Figure 2, the averaging kernel for CO retrievals between 0.2 and 4 km peaks at the representative altitudes. Therefore the CO mixing ratios in this layer can be used for this comparison. Daily averaged CO mixing ratios between 0.2 and 4 km from April 1998 to April 1999, corresponding to the period of the surface CO measurements, are shown in Figure 9. The surface CO data in Figure 9 were observed using a modified nondispersive infrared (NDIR) photometer [*Tanimoto et al.*, 2000] and are 12-hour averages of 1-hour continuous observations. The seasonal mean reference level derived from the least squaress fit to the FTIR data from May 1995 to June 2000 (excluding 1998) using equation (1) is also plotted.

[49] The retrieved CO mixing ratios between 0.2 and 4 km generally agree with the surface NDIR CO data. Both the FTIR and NDIR measurements showed significant increases in CO in the second half of 1998. The maximum enhancement of the CO mixing ratio between 0.2 and 4 km in August was about a factor of 1.7 greater than the seasonal background level. Unfortunately, on a number of days in late July, mid-September, and early October when surface CO concentrations were high (>300 ppbv), there were no FTIR measurements due to the cloudy conditions.

[50] Figure 10 shows images of the total ozone mapping spectrometer (TOMS) on board the Earth Probe spacecraft aerosol index for August 19 and 22, 1998, displaying the extent of smoke coverage. It can be seen that smoke covered a wide area over eastern Siberia near northern Japan on these days. From July to early October 1998, Earth Probe TOMS detected smoke from fires in eastern Russia (see images of the aerosol index on http://toms.gsfc.nasa.gov/). For most of this period the smoke was essentially stationary with some southeast to east movement toward northern

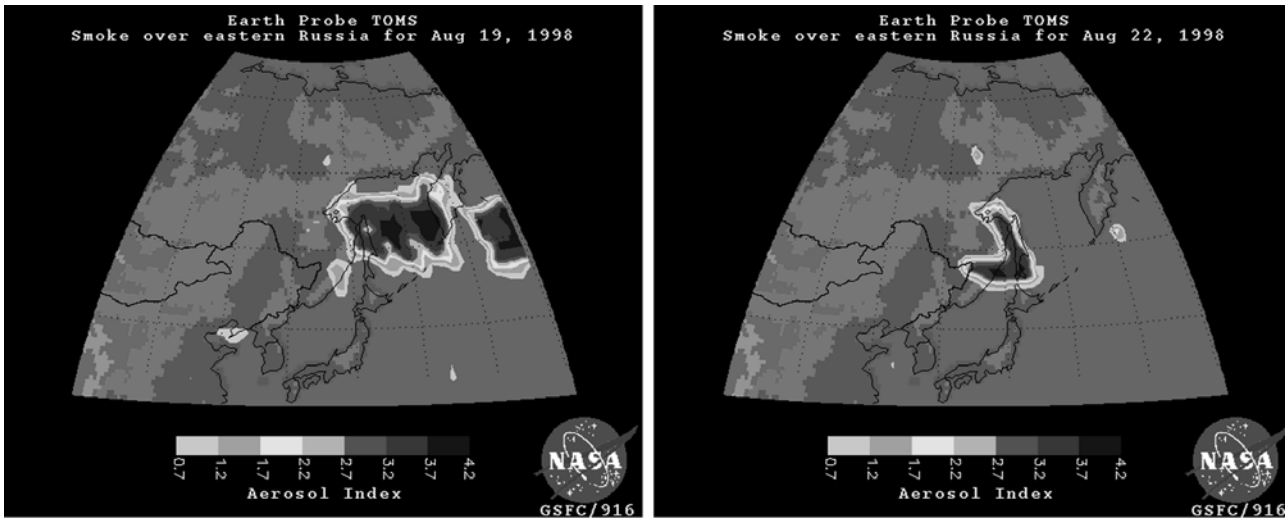

Figure 10. Images of the smoke detected by Earth Probe total ozone mapping spectrometer (TOMS) using the TOMS aerosol index on (left) 19 and (right) 22 August 1998. See color version of this figure at back of this issue.

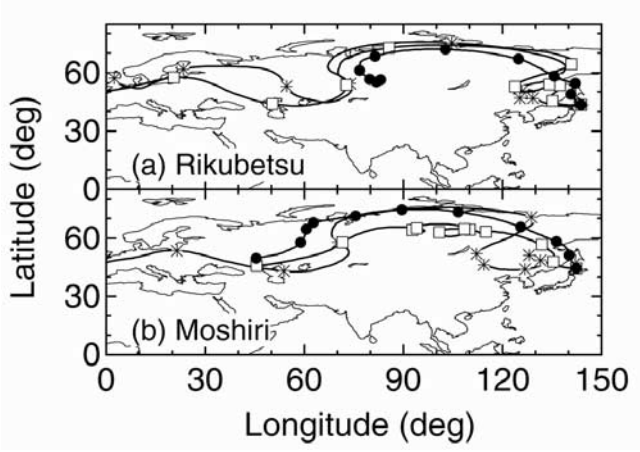

Figure 11. Kinematic 10-day back-trajectories calculated for the airmasses reaching the 300 hPa (stars), 500 hPa (open squares), and 800 hPa (solid circles) levels over (a) Rikubetsu and (b) Moshiri on 22 August 1998.

Japan (see text onhttp://toms.gsfc.nasa.gov/). This period is coincident with the enhancements of tropospheric CO, C_2H_6, C_2H_2, and HCN observed with ground-based infrared solar spectroscopy and of the surface CO observed with the NDIR instrument. It supports the hypothesis that the 1998 eastern Siberia forest fires were responsible for the abnormally high tropospheric concentrations of these molecules over northern Japan in the same period. Figures 11a and 11b show 10-day back-trajectories originating at the 300, 500, and 800 hPa levels above Rikubetsu and Moshiri on August 22, 1998. It is apparent that FTIR measurements in northern Japan on this day sampled air masses containing emissions from eastern Siberia fires (see Figures 10 and 11).

[51] Since the photochemical lifetime of HCN is longer than that of CO, the HCN/CO ratio in an airmass increases as the airmass transports. Therefore transport of the emissions is an important process for the changes in the HCN/CO ratio. It can be seen from Figure 5 that the $\Delta HCN/\Delta CO$ slope in 1998 (1.60×10^{-3}) was smaller than that in the other years (2.02×10^{-3}). This is consistent with that biomass burning intensively occurred in eastern Siberia near northern Japan in 1998. The lower $\Delta HCN/\Delta CO$ slope observed in 1998 suggested that air parcels sampled by the FTIR measurements that year was relatively "young." However, owing to the dependence of the HCN/CO emission ratio on fire type, burnt biomaterials, and the phase of the fire, these effects have to be taken into account for a more detailed study.

[52] It has been shown that significant increases in HCN above Kitt Peak occurred during the strong El Niño Southern Oscillation (ENSO) warm phases in 1982–1983 and 1997–1998 [*Rinsland et al.*, 2001]. High HCN values observed at Mauna Loa in late 1997 were also related to the ENSO events [*Rinsland et al.*, 1999]. As an ENSO phenomenon, anomalous sea-surface temperatures (SST) were observed in 1997–1998 [e.g., *McPhaden and Yu*, 1999]. Since ocean uptake is an important sink of atmospheric HCN [*Li et al.*, 2000], changes in SST would affect the strength of this sink and in turn disturb the balance between HCN sinks and sources. However, detailed discussion of the relationship between SST and the HCN sink is beyond the scope of this study.

[53] Seasonal mean anomalies in the UV irradiance observed at Santiago, Chile, between January 1992 and December 1998 showed low irradiance at 305 and 340 nm coincident with the ENSO signals [*Cabrera and Fuenzalida*, 1999]. Therefore the ENSO effects could alter the destruction processes for tropospheric CO, C_2H_6, C_2H_2, and HCN through their photochemical reactions with tropospheric OH. In addition, ENSO is associated with large-scale variations in the dynamical behavior of the global atmosphere-ocean system [*Dickey et al.*, 1999], such as convection, circulation, and air temperature, which could affect the distribution, frequency, and intensity of biomass burning emissions [*Rinsland et al.*, 1999]. Therefore the abnormally high values of tropospheric CO, C_2H_6, C_2H_2, and HCN observed in northern Japan in 1998 might be related to the 1997–1998 ENSO events.

[54] It can be seen in Figure 3d that, in addition to the abnormally high values in 1998, tropospheric HCN columns over northern Japan were also enhanced in late 1997. Since the biomass burning activity on the Asian and European continents did not seem to increase in this period (see Figure 8), fires occurring in these areas might not be the major cause of the enhanced HCN in late 1997. Enhancement of tropospheric HCN was also observed at Mauna Loa, simultaneously with high CO and C_2H_6 beginning in September 1997 with the highest levels seen in November 1997. This has been attributed to the widespread southeast Asia fires at that time [*Rinsland et al.*, 1999]. A 3-D chemical transport model shows a northward propagation of the HCN signal originating in the tropics due to biomass burning there [*Li et al.*, 2000]. Therefore part of the high HCN amounts observed in northern Japan in late 1997 were possibly due to the transport of the intensive emissions of tropical biomass burning. Moreover, unlike the case for Mauna Loa, where HCN, CO, and C_2H_6 were all enhanced in 1997, while HCN concentrations over northern Japan in late 1997 were enhanced, CO, C_2H_6, and C_2H_2 concentrations were almost at their normal levels. It implies that the airmasses containing high HCN that reached northern Japan in late 1997 had experienced a relatively long transport from the tropical regions, because the lifetime of HCN is longer than that of CO, C_2H_6, and C_2H_2.

5. Summary and Conclusions

[55] Northern Japan is an ideal place to monitor the outflow of continental air from Asia, because airmasses reaching the 300–800 hPa levels above northern Japan are primarily transported from this area. Seasonal variations in the tropospheric column amounts and mixing ratios of CO, C_2H_6, C_2H_2, and HCN were observed at Rikubetsu and Moshiri in northern Japan using ground-based infrared solar spectroscopy. Tropospheric CO, C_2H_6, and C_2H_2 reached their maximum concentrations in winter-spring and minimum concentrations in summer-fall, mainly controlled by the seasonal photochemical cycle of OH and the anthropogenic sources of these molecules. Good correlations between CO, C_2H_6, and C_2H_2 indicated that they undergo similar atmospheric dilution and production processes. Maximum and minimum values of HCN were observed in

summer and winter, respectively, mainly driven by biomass burning and ocean uptake. Deviation of tropospheric partial columns of HCN relative to its seasonal mean (ΔHCN) showed a good correlation with the similar deviation of CO (ΔCO), suggesting that increases in CO and HCN above their reference levels were due to the same source, which appears to be biomass burning.

[56] Negative trends in the tropospheric partial columns of CO, C_2H_6, and C_2H_2 were observed over northern Japan from May 1995 to June 2000 (excluding the 1998 data). Increased solar UV radiation due to the global stratospheric O_3 depletion [*Cabrera and Fuenzalida.*, 1999] and reduced emissions of CO, C_2H_6, and C_2H_2 from biomass burning and anthropogenic sources in the past decade [*Novelli et al.*, 1998] are the possible causes for the negative trends observed for these molecules.

[57] Significant enhancements of CO, C_2H_6, C_2H_2, and HCN were observed in 1998. These were consistent with increased biomass burning on the Asian continent in 1998 as seen in ATSR global fire maps. It is most likely that biomass burning in eastern Siberia from mid-July to early October resulted in the remarkably high CO, C_2H_6, C_2H_2, and HCN measured over northern Japan during the same period. This is consistent with the lower ΔHCN/ΔCO slope in 1998, suggesting that air masses sampled by the FTIR measurements in 1998 were relatively young.

[58] Abnormally high amounts of the tropospheric HCN appeared during the strong ENSO period in 1997–1998, suggesting the possibility that high HCN reaching northern Japan may have included the contribution of El Nino fires occurred in this period. Further investigation of the relationship between the ENSO phenomena and the changes in tropospheric HCN could help to provide information on the sources and sinks of HCN, which are still poorly understood.

[59] **Acknowledgments.** The authors would like to thank M. Sera, Y. Ikegami, N. Toriyama, M. Kanada, H. Jindo, S. Higuchi, K. Izumi, T. Moriyama, Y. Song, and H. Hanano for their assistance in the FTIR observations at Rikubetsu and Moshiri. They also thank H. Tanimoto, J. Hirokawa, Y. Kajii, and H. Akimoto for providing the Rishiri CO data. The kind and helpful cooperation of the town of Rikubetsu is greatly appreciated. The authors also wish to acknowledge the public use of the ATSR World Fire Atlas and the TOMS smoke images.

References

Arino, O., M. Simon, I. Piccolini, and J. M. Rosaz, The ERS-2 ATSR-2 World Fire Atlas and the ERS-2 ATSR-2 World Burnt Surface Atlas projects, in paper presented at the 8th ISPRS Conference on Physical Measurement and Signatures in Remote Sensing, Int. Soc. For Photogramm. and Remote Sens., Aussois, Jan. 8–12, 2001.

Bachmeier, A. S., R. E. Newell, M. C. Shipham, Y. Zhu, D. R. Blake, and E. V. Browell, PEM-West A: Meteorological overview, *J. Geophys. Res.*, *101*, 1655–1677, 1996.

Blake, N. J., D. R. Blake, Y. T-Chen, J. E. Collins Jr., G. W. Sachse, B. E. Anderson, and F. S. Rowland, Distribution and seasonality of selected hydrocarbons and halocarbons over the west Pacific basin during PEM-West A and PEM-West B, *J. Geophys. Res.*, *102*, 28,315–28,331, 1997.

Cabrera, S., and H. A. Fuenzalida, Interannual variations of global UV radiation in Santiago, Chile (33.5°S), *Geophys. Res. Lett.*, *26*, 2945–2948, 1999.

Chan, L. Y., C. Y. Chan, H. Y. Liu, S. Christopher, S. J. Oltmans, and J. M. Harris, A case study on the biomass burning in southeast Asia and enhancement of tropospheric ozone over Hong Kong, *Geophys. Res. Lett.*, *27*, 1479–1482, 2000.

Cicerone, R. J., and R. Zellner, The atmospheric chemistry of hydrogen cyanide, *J. Geophys. Res.*, *88*, 10,689–10,696, 1983.

Dickey, J. O., P. Gegout, and S. L. Marcus, Earth-atmospheric angular momentum exchange and ENSO: The rotational signature of the 1997–98 event, *Geophys. Res. Lett.*, *26*, 2477–2480, 1999.

Gupta, M. L., R. J. Cicerone, D. R. Blake, F. S. Rowland, and I. S. A. Isaksen, Global atmospheric distributions and source strengths of light hydrocarbons and tetrachloroethene, *J. Geophys. Res.*, *103*, 28,219–28,235, 1998.

Holzinger, R., C. Warneke, A. Hansel, A. Jordan, and W. Lindinger, Biomass burning as a source of formaldehyde, acetaldehyde, methanol, acetone, acetonitrile, and hydrogen cyanide, *Geophys. Res. Lett.*, *26*, 1161–1164, 1999.

Li, Q. L., D. J. Jacob, I. Bey, R. M. Yantosca, Y. Zhao, Y. Kondo, and J. Notholt, Atmospheric hydrogen cyanide (HCN): Biomass burning source, ocean sink?, *Geophys. Res. Lett.*, *27*, 357–360, 2000.

Logan, J. A., M. J. Prather, S. C. Wofsy, and M. B. McElroy, Tropospheric chemistry: A global perspective, *J. Geophys. Res.*, *86*, 7210–7254, 1981.

Mahieu, E., C. P. Rinsland, R. Zander, L. Delbouille, P. Demoulin, and G. Roland, Vertical column abundance of HCN deduced from ground-based infrared solar spectra: Long-term trend and variability, *J. Atmos. Chem.*, *20*, 299–310, 1995.

Mahieu, E., C. P. R. Zander, L. Delbouille, P. Demoulin, G. Roland, and C. Servais, Observed trends in total vertical column abundance of atmospheric gases from IR solar spectra recorded at the Jungfraujoch, *J. Atmos. Chem.*, *28*, 227–243, 1997.

McPhaden, M. J., and X. Yu, Equatorial waves and the 1997–98 El Niño, *Geophys. Res. Lett.*, *26*, 2961–2964, 1999.

Merrill, J. T., R. E. Newell, and A. S. Bachmeier, A meteorological overview for the Pacific Exploratory Mission-West Phase B, *J. Geophys. Res.*, *102*, 28,241–28,253, 1997.

Notholt, J., C. G. Toon, C. P. Rinsland, N. S. Pougatchev, N. B. Jones, B. J. Connor, R. Weller, M. Gautrois, and O. Schrems, Latitudinal variations of trace gas concentrations in the free troposphere measured by solar absorption spectroscopy during a ship cruise, *J. Geophys. Res.*, *105*, 1337–1349, 2000.

Novelli, P. C., K. A. Masarie, and P. M. Lang, Distributions and recent changes of carbon monoxide in the lower troposphere, *J. Geophys. Res.*, *103*, 19,015–19,033, 1998.

Pougatchev, N. S., and C. P. Rinsland, Spectroscopic study of the seasonal variation of carbon monoxide distribution above Kitt Peak, *J. Geophys. Res.*, *100*, 1409–1416, 1995.

Pougatchev, N. S., B. J. Connor, and C. P. Rinsland, Infrared measurements of the ozone vertical distribution above Kitt Peak, *J. Geophys. Res.*, *100*, 16,689–16,697, 1995.

Rinsland, C. P., A. Glodman, and G. M. Stokes, Identification of atmospheric C_2H_2 lines in the 3230–3340 cm^{-1} region of high resolution solar absorption spectra recorded at the National Solar Observatory, *Appl. Opt.*, *24*, 2044–2046, 1985.

Rinsland, C. P., R. Zander, C. B. Farmer, R. H. Norton, and J. M. Russell III, Concentration of ethane (C_2H_6) in the lower stratosphere and upper troposphere and acetylene (C_2H_2) in the upper troposphere deduced from Atmospheric Trace Molecule Spectroscopy/Spacelab 3 spectra, *J. Geophys. Res.*, *92*, 11,951–11,964, 1987.

Rinsland, C. P., N. B. Jones, B. J. Connor, J. A. Logan, N. S. Pougatchev, A. Goldman, F. J. Murcray, T. M. Stephen, A. S. Pine, R. Zander, E. Mahieu, and P. Demoulin, Northern and southern hemisphere ground-based infrared spectroscopic measurements of tropospheric carbon monoxide and ethane, *J. Geophys. Res.*, *103*, 28,197–28,217, 1998.

Rinsland, C. P., A. Goldman, F. J. Murcray, T. M. Stephen, N. S. Pougatchev, J. Fishman, S. J. David, R. D. Baltherwick, P. C. Novelli, N. B. Jones, and B. J. Connor, Infrared solar spectroscopic measurements of free tropospheric CO, C_2H_6, and HCN above Mauna Loa, Hawaii: Seasonal variations and evidence for enhanced emissions from the Southeast Asian tropical fires of 1997–1998, *J. Geophys. Res.*, *104*, 18,667–18,680, 1999.

Rinsland, C. P., E. Mahieu, R. Zander, P. Demoulin, J. Forrer, and B. Buchmann, Free tropospheric CO, C_2H_6, and HCN above center Europe: Recent measurements from the Jungfraujoch station including the detection of elevated columns during 1998, *J. Geophys. Res.*, *105*, 24,235–24,249, 2000.

Rinsland, C. P., A. Goldman, R. Zander, and E. Mahieu, Enhanced tropospheric HCN columns above Kitt Peak during the 1982–1983 and 1997–1998 El Niño warm phase, *J. Quant. Spectrosc. Radiat. Transfer*, *69*, 3–8, 2001.

Rodgers, C. D., Characterization and error analysis of profile retrieved from remote sounding measurements, *J. Geophys. Res.*, *95*, 5587–5595, 1990.

Rothman, L. S., The HITRAN molecular spectroscopic database and HAWKS (HITRAN atmospheric workstation): 1996 edition, *J. Quant. Spectrosc. Radiat. Transfer*, *60*, 665–710, 1998.

Rudolph, J., The tropospheric distribution and budget of ethane, *J. Geophys. Res.*, *100*, 11,369–11,381, 1995.

Singh, H. B., and P. B. Zimmerman, Atmospheric distribution and sources

of nonmethane hydrocarbons, in *Gaseous Pollutants: Characterization and Cycling*, edited by J. O. Nriagu, pp. 177–235, John Wiley, New York, 1992.

Singh, H. B., et al., Latitudinal distribution of reactive nitrogen in the free troposphere over the Pacific ocean in the late winter/early spring, *J. Geophys. Res.*, *103*, 28,237–28,246, 1998.

Smith, M. A. H., Compilation of atmospheric gas concentration profile from 0 to 50 km, *NASA Tech. Memo.,* TM83289, 1982.

Taalas, P., G. T. Amanatidis, and A. Heikkila, European conference on atmospheric UV radiation: Overview, *J. Geophys. Res.*, *105*, 4777–4785, 2000.

Talbot, R. W., et al., Chemical characteristics of continental outflow from Asia to the troposphere over the west Pacific ocean during September–October 1991: Results from PEM-West A, *J. Geophys. Res.*, *101*, 1713–1725, 1996.

Talbot, R. W., et al., Chemical characteristics of continental outflow from Asia to the troposphere over the west Pacific ocean during February–March 1994: Results from PEM-West B, *J. Geophys. Res.*, *102*, 28,255–28,274, 1997.

Tanimoto, H., Y. Kajii, J. Hirokawa, H. Akimoto, and N. P. Minko, The atmospheric impact of boreal forest fires in far eastern Siberia on the seasonal variation of carbon monoxide: Observation at Rishiri, a northern remote island in Japan, *Geophys. Res. Lett.*, *27*, 4073–4076, 2000.

Volz, A., D. H. Ehhalt, and R. G. Derwent, Seasonal and latitudinal variations of ^{14}CO and tropospheric concentration of OH radicals, *J. Geophys. Res.*, *86*, 5163–5171, 1981.

Yokelson, R. J., D. W. T. Griffith, and D. E. Ward, Open-path Fourier transform infrared studies of lager scale laboratory biomass fires, *J. Geophys. Res.*, *101*, 21,067–21,080, 1996.

Yokelson, R. J., R. Susott, D. E. Ward, J. Reardon, and D. W. F. Griffith, Emissions from smoldering combustion of biomass measured by open-path Fourier transform infrared spectroscopy, *J. Geophys. Res.*, *102*, 18,865–18,877, 1997.

Zander, R., C. P. Rinsland, D. H. Ehhalt, J. Rudolph, and P. Demoulin, Vertical column abundance and seasonal cycle of acetylene, C_2H_2, above the Jungfraujoch station, derived from IR solar observations, *J. Atmos. Chem.*, *13*, 359–372, 1991.

Zhao, Y., Y. Kondo, F. J. Murcray, X. Liu, M. Koike, K. Kita, H. Nakajima, I. Murata, and K. Suzuki, Carbon monoxide column abundances and tropospheric concentrations retrieved from high resolution ground-based infrared solar spectra at 43.5°N over Japan, *J. Geophys. Res.*, *102*, 23,403–23,441, 1997.

Zhao, Y., Y. Kondo, F. J. Murcray, X. Liu, M. Koike, H. Irie, K. Strong, K. Suzuki, M. Sera, and Y. Ikegami, Seasonal variations of HCN over northern Japan measured by ground-based infrared solar spectroscopy, *Geophys. Res. Lett.*, *27*, 2085–2088, 2000.

H. Irie and Y. Matsumi, Solar-Terrestrial Environment Laboratory, Nagoya University, 3-13 Honohara, Toyokawa, 442-8507, Japan. (irie@stelab.nagoya-u.ac.jp; matsumi@stelab.nagoya-u.ac.jp)

N. B. Jones, NIWA Climate, Private Bag 50061, Omakau, Lauder 9182, New Zealand. (n.jones@niwa.cri.nz)

M. Koike, Department of Earth and Planetary Sciences, Graduate School of Science, University of Tokyo, 7-3-1 Hongo, Bunkyo-ku, Tokyo 113-0033, Japan. (koike@eps.s.u-tokyo.ac.jp)

Y. Kondo, Research Center for Advanced Science and Technology, University of Tokyo, 4-6-1 Komaba, Meguro-ku, Tokyo 153-8904, Japan. (kondo@atmos.rcast.u-tokyo.ac.jp)

I. Murata, Department of Astronomy and Geophysics, Graduate School of Science, Tohoku University, Aramaki-Aoba, Sendai, 980-8578, Japan. (murata@pat.geophys.tohoku.ac.jp)

H. Nakajima and H. Nakane, National Institute for Environmental Studies (NIES), 16-2 Onogawa, Tsukuba, Ibaraki 305-0053, Japan. (hide@nies.go.jp; nakane@nies.go.jp)

C. P. Rinsland, Atmospheric Sciences Division, NASA Langley Research Center, Mail Stop 401A, Hampton, VA 23681-2199, USA. (c.p.rinsland@larc.nasa.gov)

K. Strong, Department of Physics, University of Toronto, 60 St. George Street, Toronto, ON, M5S 1A7, Canada. (strong@atmosp.physics.utoronto.ca)

K. Suzuki, Faculty of Education and Human Sciences, Yokohama National University, Hodogaya-ku, Yokohama, 240-8501, Japan. (ksuzuki@ed.ynu.ac.jp)

Y. Zhao, Mechanical and Aeronautical Engineering, University of California, One Shields Ave., Davis, CA 95616, USA. (yzhao@mae.ucdavis.edu)

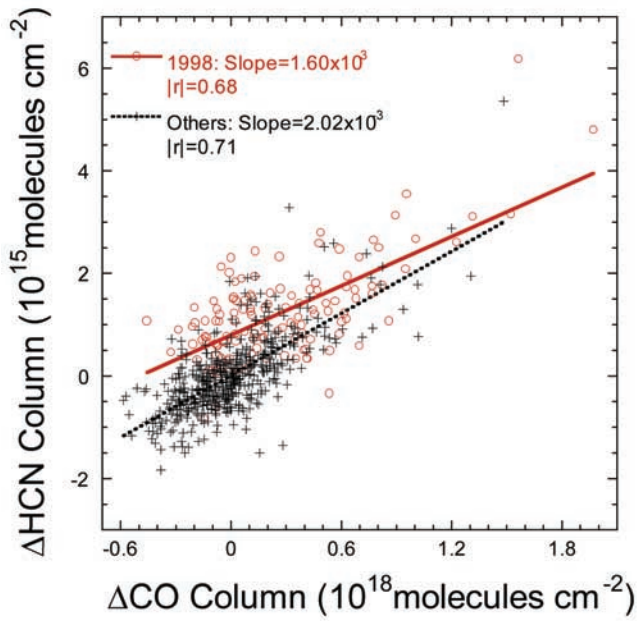

Figure 5. Correlation between ΔHCN and ΔCO. See text for details.

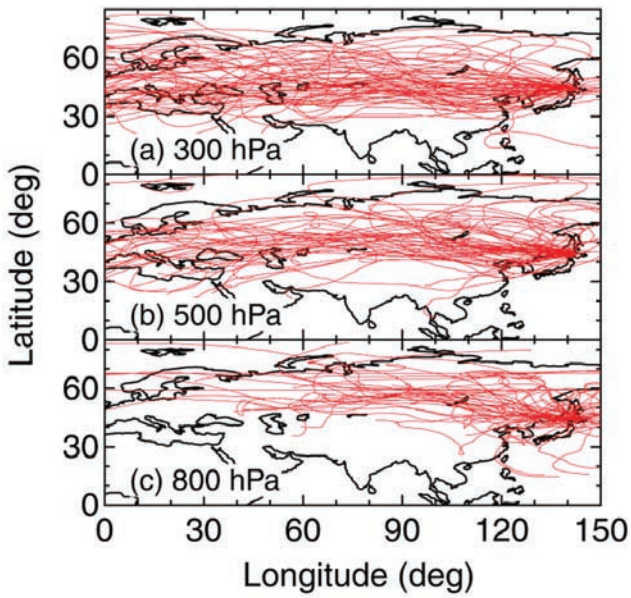

Figure 7. Kinematic 10-day back-trajectories calculated for the air masses reaching the (a) 300 hPa, (b) 500 hPa, and (c) 800 hPa levels over northern Japan.

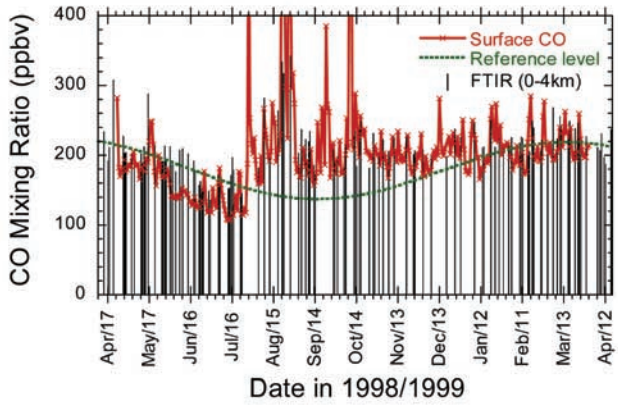

Figure 9. CO mixing ratios between 0.2 and 4 km over northern Japan from April 1998 to April 1999 retrieved from ground-based infrared solar spectra. Surface CO mixing ratios observed at Rishiri, Japan [*Tanimoto et al.*, 2000], are also shown for comparison. The dashed line represents the reference level of the seasonal mean 0.2–4 km CO mixing ratio derived from the best fit to the May 1995 to June 2000 data (excluding the 1998 period) using equation (1).

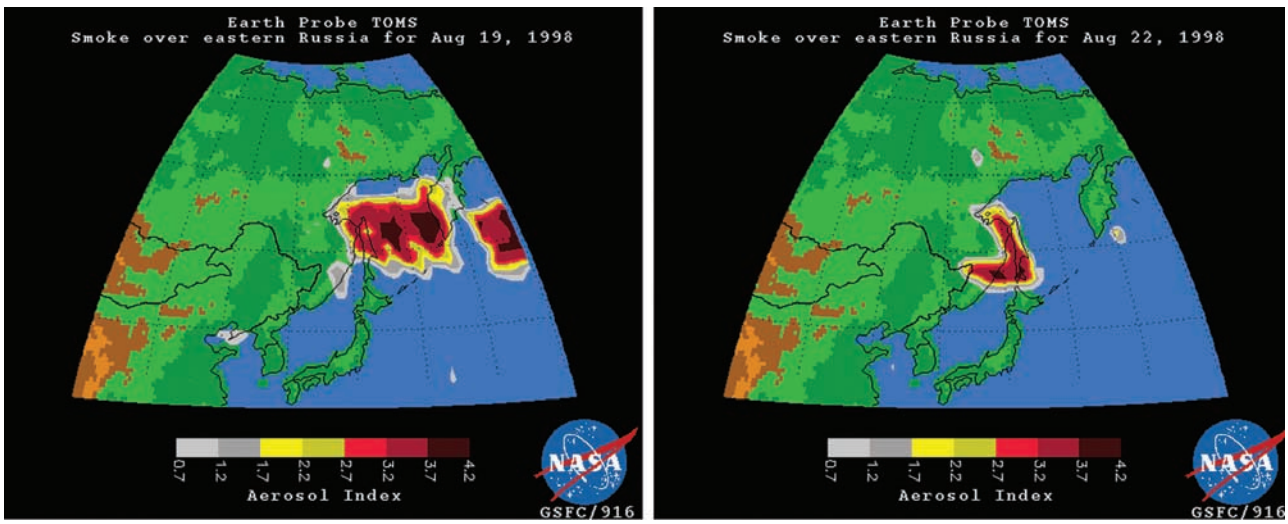

Figure 10. Images of the smoke detected by Earth Probe total ozone mapping spectrometer (TOMS) using the TOMS aerosol index on (left) 19 and (right) 22 August 1998.